

Clumping factors of HII, HeII and HeIII

Akila Jeesson-Daniel,^{1,2,3*} Benedetta Ciardi² and Luca Graziani²

¹*School of Physics, University of Melbourne, Parkville, VIC 3010, Australia*

²*Max Planck Institute for Astrophysics, Karl-Schwarzschild Straße 1, 85741 Garching, Germany*

³*ARC Centre of Excellence for All-Sky Astrophysics (CAASTRO)*

ABSTRACT

Estimating the intergalactic medium ionization level of a region needs proper treatment of the reionization process for a large representative volume of the universe. The clumping factor, a parameter which accounts for the effect of recombinations in unresolved, small-scale structures, aids in achieving the required accuracy for the reionization history even in simulations with low spatial resolution.

In this paper, we study for the first time the redshift evolution of clumping factors of different ionized species of H and He in a small but very high resolution simulation of the reionization process. We investigate the dependence of the value and redshift evolution of clumping factors on their definition, the ionization level of the gas, the grid resolution, box size and mean dimensionless density of the simulations.

Key words: radiative transfer – methods: numerical – intergalactic medium – cosmology: theory – dark ages, reionization, first stars

1 INTRODUCTION

Simulating the reionization history is a complex task due to the wide range of spatial and mass scales which must be considered (e.g. Ciardi & Ferrara 2005; Barkana & Loeb 2007; Morales & Wyithe 2010, and references therein). Due to the patchy nature of reionization, large comoving volumes ($\geq 100 h^{-1}\text{Mpc}$) are required to representatively sample the dark matter halo distribution (Barkana & Loeb 2004) and to contain the large ionized regions (typically several tens of Mpc in size) expected prior to overlap (Wyithe & Loeb 2004). Concurrently, high mass resolution is also needed to resolve the low mass galaxies thought to dominate the ionizing photon emission (e.g. Bolton & Haehnelt 2007), as well as the Lyman-limit systems which determine the ionizing photons' mean free paths during the final stages of reionization (McQuinn et al. 2007). Incorporating these sources and sinks of ionizing photons correctly into the simulations requires spatial scales of 10 kpc to be resolved (Schaye 2001; McQuinn, Oh, & Faucher-Giguère 2011).

Performing N-body simulations which include gas hydrodynamics and the multi-frequency radiative transfer (RT) of ionizing photons in a volume with the required spatial and mass resolution is therefore a Herculean task, with computational limits dictating the resolution one can achieve. To alleviate this problem, it is possible to simulate large computational volumes at a limited resolution and instead employ sub-grid prescriptions for the

physics which would be otherwise missed. A typical example in reionization simulations is the adoption of a clumping factor, a quantity which accounts for the effect of recombinations in unresolved, small-scale structures on calculations of the intergalactic medium (IGM) ionization state (e.g. Madau, Haardt, & Rees 1999; Iliev et al. 2007; McQuinn et al. 2007; Kohler, Gnedin, & Hamilton 2007).

In recent years, a significant amount of effort has therefore gone into calculating the clumping factor of gas during the epoch of reionization (e.g. Giroux & Shapiro 1996; Gnedin & Ostriker 1997; Iliev, Scannapieco, & Shapiro 2005; Trac & Cen 2007; McQuinn et al. 2007; Kohler, Gnedin, & Hamilton 2007; Pawlik, Schaye, & van Scherpenzeel 2009; Raičević & Theuns 2011; Emberson, Thomas, & Alvarez 2013; Shull et al. 2012; Finlator et al. 2012; So et al. 2014; Kaurov & Gnedin 2014). Early calculations (e.g. Gnedin & Ostriker 1997) found high values for gas clumping factors ($C_{\text{gas}} \sim 40$) approaching the end of reionization. However, more recent studies have demonstrated that there are wide variations in clumping factor values depending on how the quantity is defined and on feedback effects. Pawlik, Schaye, & van Scherpenzeel (2009) have demonstrated that photo-heating during reionization significantly reduces the clumping factor of gas ($C_{\text{gas}} \sim 3$ at $z = 6$), thus lowering the number of ionizing photons needed to balance recombinations and hence keep the universe ionized. In another study, Raičević & Theuns (2011) noted that clumping factors depend sensitively on the volume over which they are computed within a simulation. Other authors have also studied the impact of different physical

* E-mail: ajeesson@unimelb.edu.au

quantities on the determination of the clumping factor. For example, both Pawlik, Schaye, & van Scherpenzeel (2009) and Shull et al. (2012) discuss the effect of selecting a density range for computing the clumping factor, while Finlator et al. (2012) showed the importance of adopting appropriate temperature and ionization thresholds.

However, previous studies have focused on computing the clumping factor for either all the gas in the IGM or for ionized hydrogen only, while they have generally ignored the clumping factor of ionized helium. This is because the majority of large-scale reionization simulations do not follow the ionization of intergalactic helium *in addition to* hydrogen (but see e.g. Trac & Cen 2007; Pawlik & Schaye 2011). However, recent work by Ciardi et al. (2012) has demonstrated that a treatment of both hydrogen and helium using multi-frequency RT is essential for accurately computing the IGM temperature and (to a lesser extent) the H ionization structure during reionization. Future large simulations should therefore ideally follow both hydrogen and helium ionization, and unless these simulations are able to resolve all relevant scales they will need to assume appropriate clumping factors for helium as well. For this reason, in this work we present estimates of the clumping factor for ionized helium *and* hydrogen, and explore their redshift evolution simultaneously by using a suite of high resolution, multi-frequency RT simulations. We also examine in detail the quantities affecting the determination of these clumping factors, such as resolution, gas density and its distribution.

This paper is organized as follows. We begin in Section 2 where we briefly describe our radiative transfer simulations. We then examine the clumping factor and its definition in detail in Section 3. Finally, we present our conclusions in Section 4. The cosmological parameters used throughout this paper are as follows: $\Omega_{0,m}=0.26$, $\Omega_{0,\Lambda} = 0.74$, $\Omega_{0,b} = 0.024 h^{-2}$, $h=0.72$, $n_s=0.95$ and $\sigma_8=0.85$, where the symbols have their usual meaning.

2 SIMULATIONS OF REIONIZATION

The reionization simulations used here are based on those recently described in detail by Ciardi et al. (2012). In this work, we shall therefore only summarize their main characteristics. Our reionization simulations are performed by post-processing high resolution cosmological hydrodynamical simulations with the 3D RT grid based Monte Carlo code **CRASH** (Ciardi et al. 2001; Maselli, Ferrara, & Ciardi 2003; Maselli, Ciardi, & Kanekar 2009; Pierleoni, Maselli, & Ciardi 2009; Partl et al. 2011; Graziani, Maselli, & Ciardi 2013). The hydrodynamical simulations are performed with the tree-smoothed particle hydrodynamics code **GADGET-3**, which is an updated version of the publicly available code **GADGET-2** (Springel 2005). Haloes are identified at each redshift in the cosmological simulations using a friends-of-friends algorithm with a linking length of 0.2. The hydrodynamical simulation snapshots – which are sampled at regular redshift intervals – therefore provide the initial IGM gas distribution and halo masses. These quantities are then transferred to a uniform Cartesian grid of N_c^3 cells as input for **CRASH**. It should be noted that the hydrodynamic simulations do not include a self-consistent treatment of radiative feed-

back, which is shown to cause a pressure smoothing of the gas and a reduction of the clumping factor (see e.g. Pawlik, Schaye, & van Scherpenzeel 2009). Instead, an approximation of the heating of the IGM due to reionization is simulated by including an instantaneous photoionization and reheating by a spatially uniform ionizing background (Haardt & Madau 2001) assuming an optically thin IGM. In this work, we use hydrodynamical simulations performed in boxes of comoving size 8.8, 4.4 and 2.2 h^{-1} Mpc. The parameters of these simulations are summarized in Table 1. It should be noted that, although the procedure to run the simulations is the same as the one described in detail in Ciardi et al. (2012), here the size of the boxes is smaller.

Following the regridding of the hydrodynamical simulation data, the RT is then calculated as a post-process using **CRASH**, which self-consistently follows the evolution of the hydrogen and helium (92 and 8 per cent abundance by number, respectively) ionization states, along with the gas temperature. All the simulation boxes are gridded to an $N_c^3 = 128^3$ RT grid, which leads to a lower spatial resolution for the larger boxes. To study the effect of varying spatial resolution for the same box size, we therefore also simulate the 2.2 h^{-1} Mpc box with coarser grid sizes of 64^3 (2.2G64) and 32^3 (2.2G32). To test whether our gridding resolves the gas density distribution, we have also gridded the hydrodynamical simulation data to 256^3 (2.2G256), 384^3 (2.2G384) and 448^3 (2.2G448) grid sizes. Due to the time required to run **CRASH** on grid sizes above 128^3 , the highest resolution for which we have a full RT simulation (i.e. from $z \sim 15$ to $z \sim 2$) is 2.2G128, while the others have been used for testing purposes only. Furthermore, to understand the effect of varying box size for the same spatial resolution, we have performed a 64^3 simulation in the 4.4 h^{-1} Mpc box, which has the same spatial resolution as 2.2G32 and 8.8G128.

All the RT simulations start at $z = 15$ and are run until $z = 2.2$. The emission properties of the sources are derived assuming that the total comoving hydrogen ionizing emissivity at each redshift is given by equation 3 in Ciardi et al. (2012), and that the emissivity of each source is proportional to its gas mass. The advantage of this empirical approach to assigning the ionization rate is that it avoids assuming an escape fraction of ionizing photons, an efficiency of star formation and a stellar initial mass function, which are very uncertain quantities. Note, however, that we still need to assume an ionizing spectrum for the sources.

Although we expect an evolution in redshift, with a predominance of sources with harder spectra at lower redshift (e.g. Haardt & Madau 2012), in this work, following Ciardi et al. (2012), we have instead taken a simpler approach and chosen a fixed power-law spectrum for the sources at all redshifts with an extreme-UV index of $\alpha = 1.8$, which is typical of the hard spectra associated with quasars (Telfer et al. 2002). Simulation performed with this power-law spectrum is consistent with constraints on the HI photoionization rate from Ly α forest at $z \sim 6$ (Bolton & Haehnelt 2007) and the Thomson scattering optical depth (Komatsu et al. 2011) in the 35 h^{-1} Mpc box simulations of Ciardi et al. (2012). Their requirement was that HI reionization is largely completed by $z \sim 6$, consistent with observations of the HI Gunn-Peterson trough (e.g. Fan et al. 2006; Bolton & Haehnelt 2007), and HeII reionization is largely completed by $z \sim 3$. In our small volume of

Table 1. The hydrodynamical simulations used in this work. The columns list, from left to right, the simulation identifier, the comoving box size L , the total number of particles (DM and gas), the DM particle mass m_{DM} , the gas particle mass m_{gas} , the comoving softening length η , the sampling grid size N_c^3 , the sampling cell comoving size L_c and with/without RT outputs.

Model	L [h^{-1} Mpc]	Particles	m_{DM} [$h^{-1} M_{\odot}$]	m_{gas} [$h^{-1} M_{\odot}$]	η [h^{-1} kpc]	N_c^3	L_c [h^{-1} kpc]	RT
8.8G128	8.78	2×256^3	1.03×10^7	5.19×10^5	1.14	128^3	68.75	Y
4.4G128	4.39	2×256^3	1.29×10^6	6.48×10^4	0.57	128^3	34.38	Y
4.4G64	4.39	2×256^3	1.29×10^6	6.48×10^4	0.57	64^3	68.75	Y
2.2G448	2.20	2×256^3	1.61×10^5	8.10×10^3	0.29	448^3	4.91	N
2.2G384	2.20	2×256^3	1.61×10^5	8.10×10^3	0.29	384^3	5.73	N
2.2G256	2.20	2×256^3	1.61×10^5	8.10×10^3	0.29	256^3	8.59	N
2.2G128	2.20	2×256^3	1.61×10^5	8.10×10^3	0.29	128^3	17.19	Y
2.2G64	2.20	2×256^3	1.61×10^5	8.10×10^3	0.29	64^3	34.38	Y
2.2G32	2.20	2×256^3	1.61×10^5	8.10×10^3	0.29	32^3	68.75	Y

$2.2 h^{-1}$ Mpc, though, due to the presence of high density regions which lead to higher recombination rates, the volume averaged ionization level of HII is 0.91 at $z \sim 6$, and reaches 0.99 only at $z \sim 4$. HeII reionization, instead, is at 65 per cent volume averaged ionization level by $z = 2.2$. It should be noted that, despite being arbitrary, this choice assures that the requirements mentioned above are met in a large representative volume of the universe.

A preliminary exploration of the effects of varying the power-law spectral index α shows that, as expected, its value can affect both the ionization history of the various species and their clumping factors. If the volume average emissivity remains constant, a value of α in the range 1 – 3 results in very similar H reionization histories, while the effect on the evolution of HeII and HeIII is stronger because of the variation on the number of ionizing photons above 24.6 eV and 54.4 eV (refer to Ciardi et al. 2012 for more details). Therefore, for different α , the clumping factors of HII remain very similar, while those for HeII and HeIII are more strongly affected. We defer to future work a more detailed discussion of the effect of different source populations on the clumping factors.

Here, we want to stress that the main aim of this paper is to study the evolution of the clumping factor of the various species and its dependence on a number of quantities, rather than properly model the reionization process (for which our simulation volumes are far too small). For this reason, we have maintained the same emission properties of the sources for all the simulations, while we plan to investigate the effects of the redshift evolution of emission properties in future work. For the purposes of this investigation then, the detailed reionization history of the simulations is not critical. Nevertheless, for the sake of clarity, in Fig. 1 we plot the redshift evolution of the volume averaged ionization fractions of HII, HeII and HeIII in 2.2G128. x_{HII} increases steadily to $z = 8$ and then slowly flattens out with the box reaching almost full ionization. A similar behaviour at $z > 8$ is observed also in x_{HeII} and x_{HeIII} , while the shape of the curves at lower redshift is determined by the shape of the emissivity (see also fig. 1 in Ciardi et al. 2012). At $z < 6$ x_{HeII} (x_{HeIII}) starts decreasing (increasing) as more HeII is converted to HeIII.

In the next section, we will investigate the clumping factors and their dependences in more detail, using as a reference simulation (unless otherwise noted) 2.2G128.

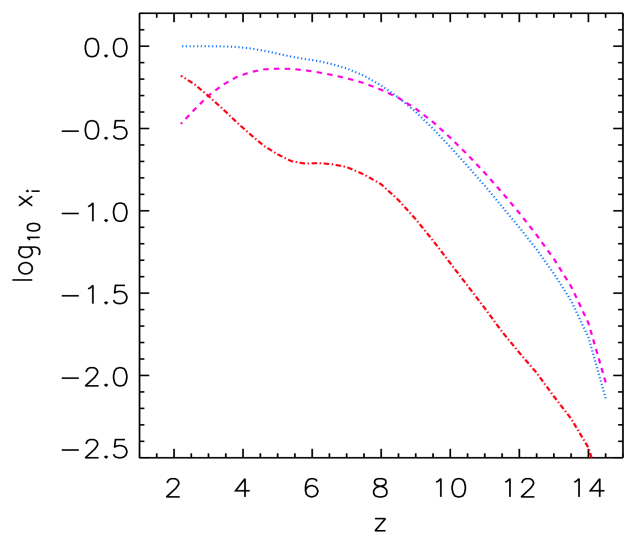


Figure 1. Redshift evolution of the volume averaged ionization fraction x_i of different species in the 2.2G128 simulation. The lines refer to: $i = \text{HII}$ (blue dotted line), HeII (magenta dashed line) and HeIII (red dot dashed line).

3 CLUMPING FACTOR

In grid based simulations of reionization with the gas made of only H, the ionization balance averaged over a cell can be written as (e.g. Kohler, Gnedin, & Hamilton 2007):

$$\frac{d}{dt} \langle n_{\text{HI}} \rangle_{\text{cell}} = -3H \langle n_{\text{HI}} \rangle_{\text{cell}} - C_{\text{I,HI}} \langle n_{\text{HI}} \rangle_{\text{cell}} \langle \dot{n}_{\gamma} \rangle_{\text{cell}} + C_{\text{R,HII}} \langle \alpha_{\text{R,HII}} \rangle_{\text{cell}} \langle n_{\text{e}} \rangle_{\text{cell}} \langle n_{\text{HII}} \rangle_{\text{cell}} \quad (1)$$

where n_{HI} and n_{HII} are the number density of neutral and ionized hydrogen, n_{e} is the number density of electrons, H is the Hubble parameter, \dot{n}_{γ} is the ionizing photon rate and $\alpha_{\text{R,HII}}$ is the recombination coefficient for HII. The angle brackets represent the mean value of the distribution the cell volume would have, if the spatial resolution were enough to resolve IGM structures down to the smallest relevant scales. $C_{\text{I,HI}} = \langle n_{\text{HI}} \dot{n}_{\gamma} \rangle_{\text{cell}} / \langle n_{\text{HI}} \rangle_{\text{cell}} \langle \dot{n}_{\gamma} \rangle_{\text{cell}}$ is the clumping factor of HI and $C_{\text{R,HII}} = \langle \alpha_{\text{R,HII}} n_{\text{e}} n_{\text{HII}} \rangle_{\text{cell}} / \langle \alpha_{\text{R,HII}} \rangle_{\text{cell}} \langle n_{\text{e}} \rangle_{\text{cell}} \langle n_{\text{HII}} \rangle_{\text{cell}}$ is the clumping factor of HII. These can be used to estimate

the ionization and recombination rates in the cell due to unresolved small scale high density regions.

In this work, we want to calculate clumping factors of the IGM for the ionized species of H and He within our simulation box such that future work can use cell sizes equivalent to our box size while using clumping factors. Even though our best gridding resolution is poorer than the spatial resolution of the hydrodynamical simulation (see Section 3.3.1), we aim to use our current simulations at limited resolution to calculate an estimate of He and H clumping factors and understand the degrees to which various factors, such as grid size, box size and overdensity of the region, would affect them.

Previous work have used a large number of equivalent definitions of clumping factors with different cuts in density ranges, ionization thresholds and with/without the effect of temperature on the recombination rates. To understand the effect of each of these modifications on the estimated clumping factor values, we start by starting from a simple definition of clumping factor and slowly progress to more complicated but accurate estimates of the true recombination number of each species.

As we are only interested in the clumping factor of the IGM, we need to remove the cells containing collapsed haloes and large dimensionless densities. We define the gas dimensionless density as

$$\Delta = n_{\text{gas}} / \langle n_{\text{gas}} \rangle, \quad (2)$$

where n_{gas} is the gas number density in a cell and $\langle n_{\text{gas}} \rangle$ is the mean gas number density of the universe at that redshift. The angle brackets $\langle \rangle$ give the value averaged within our box. This notation will be adopted throughout the paper, unless otherwise noted. The dimensionless density of a collapsed dark matter halo depends on the definition used to compute its virial radius. For example, for spherical top hat collapse the dark matter dimensionless density at the virial radius is ~ 178 (e.g. Padmanabhan 1993), while for an isothermal collapse it is ~ 60 (e.g. Lacey & Cole 1994). For comparison and consistency with earlier works, we adopt the generally used dimensionless density threshold of 100, assuming that the IGM is composed only of cells with $\Delta \leq 100$ (Miralda-Escudé, Haehnelt, & Rees 2000; Pawlik, Schaye, & van Scherpenzeel 2009; Raićević & Theuns 2011).

Our first definition of the clumping factor of a species is as follows:

$$C_i = \langle n_i^2 \rangle / \langle n_i \rangle^2, \quad (3)$$

where n_i is the number density of the species $i = \text{HII}, \text{HeII}, \text{HeIII}$ and total gas. This definition gives an estimate of the uniformity in the distribution of each species by providing the spread in the number density of species i with respect to the mean value calculated for the whole simulation volume. These clumping factors can be used e.g. in a one-zone model for reionization where the recombination term in the ionization balance equation is given by $C_i \langle n_i \rangle^2$.

Even though the above definition of C_{HII} is not very accurate considering that our gas conditions are different from the assumption in $C_{\text{R,HII}}$. Nevertheless, since most of the electrons come from H, the HII clumping factor does not change substantially by including a more accurate evaluation of n_e . The case B recombination rates vary only by a

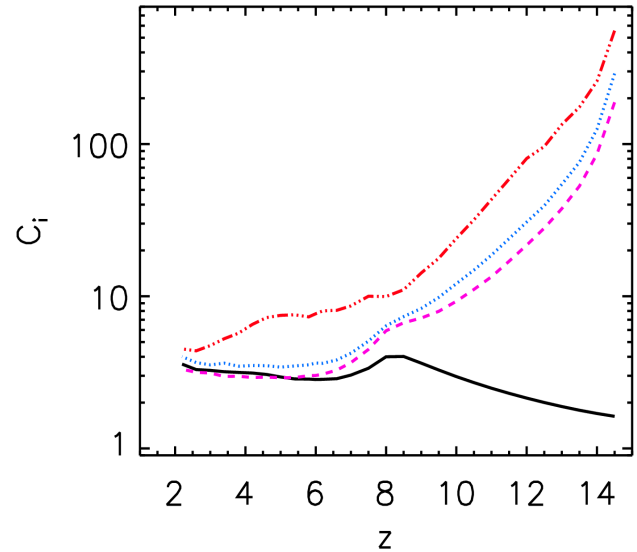


Figure 2. Clumping factor C_i of different species in the 2.2G128 simulation. The lines refer to: gas (black solid line), HII (blue dotted line), HeII (magenta dashed line) and HeIII (red triple dot dashed line).

factor of a few for temperatures above 10^4 K. We thus expect $C_{\text{HII}} \sim C_{\text{R,HII}}$ also in our simulations. This holds true even for HeII and HeIII, as the main source of electrons is mostly H (with electrons from He contributing mainly to the highly ionized regions up to about 17 percent in number) and the recombination rates of HeII and HeIII on temperature vary by only within about 4-5 times within the ionized regions in the IGM. Therefore, this definition provides a basic estimate of the clumping factors. The detailed effect due to variations in electron density and recombination rates on the clumping factors is explored in Section 3.2.

We start with studying how different species clump in our simulation 2.2G128, by calculating the redshift evolution of the clumping factor for total gas, HII, HeII and HeIII, which are shown in Fig. 2. As previous works (e.g. Pawlik, Schaye, & van Scherpenzeel 2009) typically compute the gas clumping factor, C_{gas} , this is what we analyse first. Clumping factor for total gas, C_{gas} , helps us understand the variation in the underlying gridded gas distribution in our simulation. We find that C_{gas} increases with decreasing redshift from 1.5 at $z \sim 15$ to about 3 at $z \sim 8$. This trend is due to the self-gravity of the gas in the IGM. At $z = 9$ the hydrodynamical simulation includes instantaneous photoionization and reheating of the IGM by a spatially uniform ionizing background (Haardt & Madau 2001) assuming an optically thin IGM. This feedback leads to pressure smoothing of the gas and to a reduction of the clumping factor (e.g. Pawlik, Schaye, & van Scherpenzeel 2009), which decreases to about 2 at $z \sim 6$. At $z \leq 6$ self-gravity becomes dominant again and the gas clumping factor increases to 3 at $z \sim 2$. Note that the values of C_{gas} depend on the box size and the grid size of the simulation under study (in this case 2.2G128), the effects of which will be discussed in detail in Section 3.3.

Next we focus on the clumping factors of the ionized species $i = \text{HII}, \text{HeII}$ and HeIII , which take into account

the effects of RT on the gridded gas distribution. In Fig. 2, C_{HII} reaches values as high as ~ 100 at $z \sim 14$, when only a handful of small ionized bubbles are present. Such values are obtained mainly because of the small fraction of ionized cells (i.e. with $n_{\text{HII}} > 0$) in the simulation volume and can be understood if one thinks about C_{HII} as representing the spread in the values of n_{HII} within the ionized cells (which is relatively large), divided by the fraction of ionized cells (which is very small). When the reionization process is more advanced, lower HII clumping factor values are found. Eventually, C_{HII} converges to C_{gas} at $z < 5$, when the volume averaged ionization fraction is $x_{\text{HII}} \gtrsim 0.95$. When the fraction of ionized cells approaches 1, i.e. all cells have $n_{\text{HII}} > 0$, C_{HII} represents the scatter in the n_{HII} values in the whole volume (which now is small because most cells are fully ionized).

C_{HeII} closely follows the evolution of C_{HII} , but with slightly lower values, due to the larger sizes of the HeII bubbles compared to the corresponding HII regions. This is due to a combination of the higher ionization cross-section of HeI compared to that of HI (Osterbrock 1989) and the lower number density of He atoms (about 8.5 percent of the nuclei) in the gas compared to H, although this effect is partially balanced by the lower source photon rate at 24.6 eV compared to that at 13.6 eV (~ 29 percent). On the other hand, due to the low ionizing photon rate at 54.4 eV (for the assumed spectrum this is $\sim 8\%$ of the H ionizing photon rate) and high recombination rate (i.e. ~ 5 times the one of HII), HeIII is confined to small bubbles in the vicinity of the sources. Even at $z = 2.2$, HeII reionization is not fully complete and only 65% of He is in HeIII state, while the rest is HeII. Therefore, due to the highly spatially inhomogeneous distribution of HeIII, C_{HeIII} has values higher than C_{HeII} and C_{HII} , while the qualitative redshift evolution is similar for all the three clumping factors. We should note that, while we expect the same qualitative behaviour for different choices of the source spectrum, the quantitative results are bound to change.

3.1 Dependence on ionization level

Earlier, we calculated the clumping factor C_i including all cells, independently from their ionization level. We saw that this leads to large values of the clumping factors at high redshift because of the small fraction of ionized cells and the relatively wide range in n_i . Typically, though, the clumping factor is employed to estimate the excess recombinations within the under resolved ionized volumes compared to those computed using the mean n_i of such volumes. Therefore, removing the cells with $n_i = 0$ by using ionization thresholds would give a better estimate of the clumping factors. For this reason, we also calculate the clumping factors of the different ionized species above a given ionization threshold x_{th} ,

$$C_{i,x_{\text{th}}} = \langle n_i^2 \rangle_{x_i > x_{\text{th}}} / \langle n_i \rangle_{x_i > x_{\text{th}}}^2 \quad (4)$$

where $x_i > x_{\text{th}}$ denotes the set of cells with ionization of a species i greater than x_{th} . Since the number of recombinations depends on the square of n_i , the highest contribution to the clumping factors is given by the highly ionized, dense regions.

In Fig. 3, we plot the redshift evolution of $C_{i,x_{\text{th}}}$ for

$i = \text{HII}, \text{HeII}, \text{HeIII}$ and for $x_{\text{th}} = 0, 0.1, 0.5, 0.9$, together with C_{gas} for comparison. $C_{i,0}$ is the same as C_i in Fig. 2. All species exhibit a decline in clumping factor values at high redshift when an ionization threshold $x_{\text{th}} > 0$ is introduced. This was expected as cells with $n_i = 0$ are now removed from the calculation, inducing a reduction in the range of n_i values. Note that, in general, the probability distribution function of the selected n_i becomes more peaked and less broad with increasing threshold values, leading to lower $C_{i,x_{\text{th}}}$.

$C_{\text{HII},x_{\text{th}}}$ for $x_{\text{th}} > 0$ is in the range 2.5 – 4 at $z > 8$, with $C_{\text{HII},0.1}$ about 0.25 times larger than $C_{\text{HII},0.5}$ and $C_{\text{HII},0.9}$. At $z < 8$, the curves tend to converge as most of the volume is fully ionized. $C_{\text{HeII},x_{\text{th}}}$ has a trend similar to that of $C_{\text{HII},x_{\text{th}}}$, with a larger difference (about 0.5) at $z > 8$ between the curves for $x_{\text{th}} > 0$. At redshifts $z < 6$, $C_{\text{HeII},0.1}$ and $C_{\text{HeII},0.5}$ are lower than C_{gas} as these thresholds select a smaller range of cell densities. It is interesting to note that at $z < 4$, $C_{\text{HeII},0.9}$ starts increasing because the number of cells with $x_{\text{HeII}} > 0.9$ decreases dramatically as more and more HeII atoms are converted to HeIII close to the ionizing sources. At $z < 3$, the curve is noisy, as less than 1 per cent of the cells have $x_{\text{HeII}} > 0.9$, with only 757 (18) cells satisfying the criterion at $z \sim 2.2$ (2.0).

The curves for HeIII show similar values and trends, albeit noisier, as the reionization of HeII to HeIII is a slow and inhomogeneous process which is dominated by the high density regions around the sources, where two competing processes sculpt the reionization structure of HeIII - the ionization of the gas by sources and the fast recombination of HeIII to HeII. There are very few cells with very high ionization. As a reference, less than 0.2 (10) percent of the cells have $x_{\text{HeIII}} > 0.9$ at $z = 4.5$ (2.2), and even at $z = 2.2$, 90 per cent of the cells have $0.1 < x_{\text{HeIII}} < 0.9$. This leads to very noisy clumping factors, especially with high ionization thresholds. For $x_{\text{th}} = 0.5$ and 0.1, the clumping factors have a more complex behaviour as the range of cells crossing these thresholds is larger. The clumping factors increase until $z = 5$ and then they start decreasing as the ionization becomes more uniform, reducing the range of the selected n_{HeIII} values used to compute the clumping factors.

In general the trend is that clumping factors decrease with increasing ionization threshold. It should be kept in mind though that these clumping factors are calculated under the assumption that the recombination factor is constant, where as in reality it depends on the temperature. This dependence is explored in the next section.

3.2 Dependence on temperature-dependent recombination coefficients

A better estimate of the clumping factors within an ionized volume is obtained by using the definition of Kohler, Gnedin, & Hamilton (2007), as it takes into account also the information in the electron number density n_e and the temperature-dependent recombination rate $\alpha_{\text{R},i}$ in each cell. In this case, the clumping factor, $C_{\text{R},i,x_{\text{th}}}$, is defined as:

$$C_{\text{R},i,x_{\text{th}}} = \langle \alpha_{\text{R},i} n_e n_i \rangle_{x_i > x_{\text{th}}} / \langle \alpha_{\text{R},i} \rangle_{x_i > x_{\text{th}}} \langle n_e \rangle_{x_i > x_{\text{th}}} \langle n_i \rangle_{x_i > x_{\text{th}}} \quad (5)$$

for different ionized species HII, HeII and HeIII, at ionization thresholds $x_{\text{th}} = 0.1, 0.5, 0.9$.

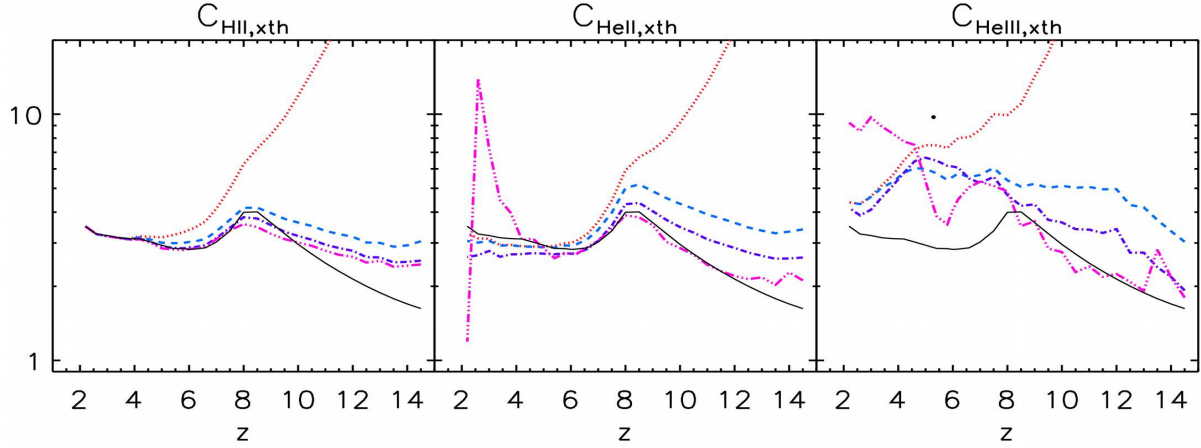


Figure 3. Clumping factors $C_{i,x_{th}}$ against redshift for different ionization thresholds in the 2.2G128 simulation. The different species plotted are (from left to right) HII, HeII and HeIII. The ionization thresholds are $x_{th} = 0$ (red dotted line), 0.1 (blue dashed line), 0.5 (purple dot dashed line), 0.9 (magenta triple dot dashed line). The C_{gas} line is plotted in all the panels as a reference (solid black line).

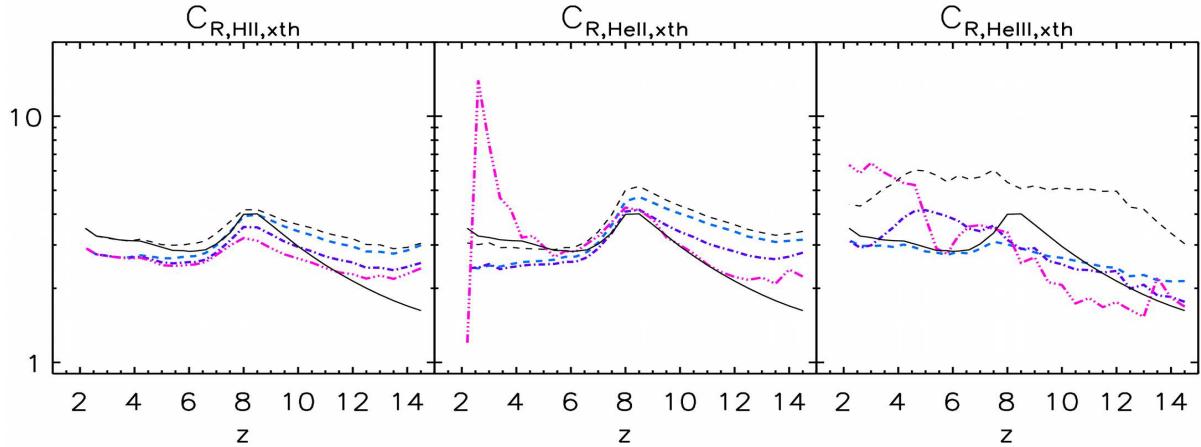


Figure 4. Clumping factors $C_{R,i,x_{th}}$ against redshift for different ionization thresholds x_{th} in the 2.2G128 simulation. The species plotted are (from left to right) HII, HeII and HeIII. The ionization thresholds are 0.1 (blue dashed line), 0.5 (purple dot dashed line), 0.9 (magenta triple dot dashed line). C_{gas} (black solid line) and $C_{i,0.1}$ (black dashed line) are plotted in all the panels as a reference.

Note that the effect of overdensity of the bubble regions in the ionization balance equation is also valid here.

Fig. 4 shows the redshift evolution of $C_{R,i,x_{th}}$ for the different ionization threshold x_{th} curves for $i = \text{HII}, \text{HeII}$ and HeIII . Also shown in each panel are the curves for C_{gas} and $C_{i,0.1}$ for reference. Starting with HII, it is easy to see that $C_{R,\text{HII},x_{th}}$ shows the same dependence of $C_{\text{HII},x_{th}}$ on x_{th} , i.e. the clumping factor decreases with increasing x_{th} . $C_{R,\text{HII},x_{th}}$, though, has values lower than $C_{\text{HII},x_{th}}$ due to highly ionized cells with higher temperatures, and thus lower recombination rates $\alpha_{R,\text{HII}}$ than the mean in the volume. At low redshifts, this effect leads to a value of $C_{R,\text{HII},x_{th}}$ which is lower than both $C_{\text{HII},x_{th}}$ and C_{gas} by about 0.5.

$C_{R,\text{HeII},x_{th}}$ and $C_{R,\text{HeIII},x_{th}}$ show a behaviour very similar to that of $C_{\text{HeII},x_{th}}$ and $C_{\text{HeIII},x_{th}}$, respectively, with the former values being slightly lower due to the effect of temperature on $\alpha_{R,\text{HeII}/\text{HeIII}}$. This effect is stronger for HeIII, as, for example, $C_{R,\text{HeIII},0.1}$ is almost half $C_{\text{HeIII},0.1}$.

Although the changes observed compared to $C_{i,x_{th}}$ are mainly due to the effect of temperature-dependent recombi-

nation rates, also accounting for the contribution from both H and He to the electron number density affects the final results. The relative importance of a correct evaluation of $\alpha_{R,i}$ and n_e depends on the species considered and on redshift. While for HII and HeII the effect of $\alpha_{R,\text{HII}/\text{HeII}}$ is dominant, for HeIII the changes induced by n_e are more relevant, although both n_e and $\alpha_{R,\text{HeIII}}$ reduce the value of the clumping factor. As an illustrative example, on average, $C_{\text{HeIII},0.1}$ is reduced by changes in $\alpha_{R,\text{HeIII}}$ alone by about 22% compared to $C_{R,\text{HeIII},0.1}$, while changes in n_e alone induce reductions of about 33%. If they are considered together the reduction is 45%.

3.3 Resolution Tests

In this sub-section, we investigate how the behaviour of the clumping factor is affected by the box and grid size, by performing a number of resolution tests.

The impact of grid and box size is due to two factors. The first one is the recombination of the species in the cells,

i.e. the larger rate of recombinations in the high density cells of a simulation with a higher resolution. The second is the source properties in a simulation volume of a given box size, i.e. larger boxes have higher mass sources which emit a higher number of ionizing photons into the surrounding IGM; this impacts the topology of reionization (refer to Appendix A for a detailed analysis), although the volume averaged emissivity is the same by construction for all simulations. Therefore, while using clumping factors in simulations to achieve better accuracy, we need to take into account both the box size and the grid size of the volume used to compute them.

3.3.1 Dependence on Grid Size

Hydrodynamic simulations have a spatial resolution equal to the softening length of the simulation. On the other hand, the resolution of the RT calculation is determined by the sampling grid size, which we have limited to 128^3 cells for our reference simulations. This leads to a lower spatial resolution in the RT calculations. To understand the effect this has on the clumping factor calculations, we compare simulations 2.2G448, 2.2G384, 2.2G256, 2.2G128, 2.2G64 and 2.2G32, which have the same hydrodynamic simulation outputs, but different sampling grid size.

The top panel of Fig. 5 shows the evolution of C_{gas} for 2.2G448, 2.2G384, 2.2G256, 2.2G128, 2.2G64 and 2.2G32. We also plot the C_{100} curve of *r9L6N256* simulation of Pawlik, Schaye, & van Scherpenzeel (2009) and the C_{100} for the *B2* simulation of Emberson, Thomas, & Alvarez (2013) for comparison.

We can see that our C_{gas} values from the $2.2 h^{-1}\text{Mpc}$ simulation converge at all redshifts for grid sizes above 384^3 cells, while the gridded gas distribution is resolved at lower redshifts also with coarser grids. In our default simulation with grid size of 128^3 , C_{gas} is resolved at $z < 7$.

Our C_{gas} values from 2.2G128 are comparable to the curve from Pawlik, Schaye, & van Scherpenzeel (2009). But even C_{gas} from 2.2G384 lies well below the estimate from Emberson, Thomas, & Alvarez (2013). This shows that even though a grid size of 384^3 is enough to resolve the gas distribution within the simulation volume, the spatial resolution of the $2.2 h^{-1}\text{Mpc}$ simulation with 256^3 gas particles is not enough to capture the unheated IGM (Jeans mass $\sim 10^4 M_{\odot}$) at high redshifts. Emberson, Thomas, & Alvarez (2013) find that a box size greater than 1 Mpc is needed, to sample the variance, along with a high mass resolution to resolve the $10^4 M_{\odot}$ gas clumps with at least 100 particles. Our highest resolution simulation has a gas particle mass of $\sim 10^4 M_{\odot}$, explaining the lower values found for C_{gas} . Once the IGM gas is heated to 10^4 K , the Jeans mass becomes $\sim 10^8 M_{\odot}$ and is easily resolved in our $2.2 h^{-1}\text{Mpc}$ simulation, although a direct comparison to Emberson, Thomas, & Alvarez (2013) is not feasible as their simulations do not include heating of the gas due to reionization. The discrepancy observed at $z < 9$ between our C_{gas} and the value from Pawlik, Schaye, & van Scherpenzeel (2009) is due to the different strength of feedback effects which blow gas out from galaxies and to the low mass resolution of their simulation, as discussed in their paper.

In the bottom three panels of Fig. 5, we plot the redshift evolution of $C_{\text{R},i,0.1}$ for $i = \text{HII}, \text{HeII}$ and HeIII for 2.2G128,

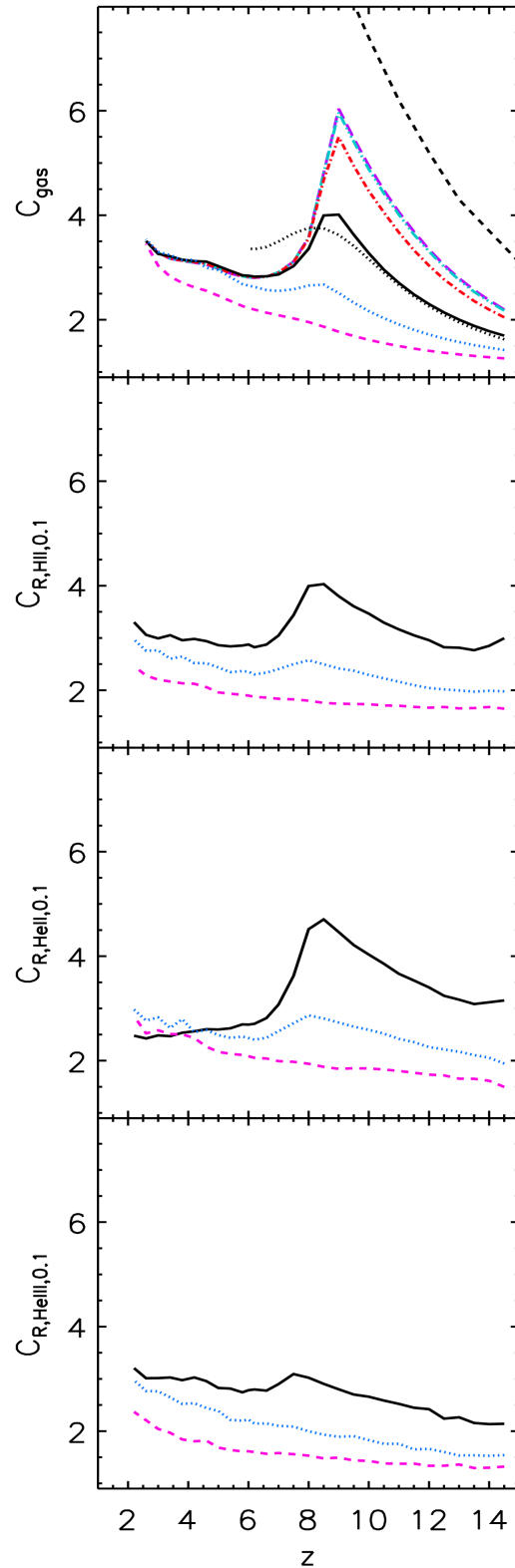


Figure 5. Redshift evolution of the clumping factor C_{gas} and $C_{\text{R},i,0.1}$ for $i = \text{HII}, \text{HeII}$ and HeIII for the simulations 2.2G448 (purple long dashed line), 2.2G384 (cyan triple dot dashed line), 2.2G256 (red dot dashed line), 2.2G128 (black solid line; reference), 2.2G64 (blue dotted line) and 2.2G32 (magenta dashed line). Also, plotted for comparison are the C_{100} curve of *r9L6N256* simulation of Pawlik, Schaye, & van Scherpenzeel (2009) (black dotted line) and the C_{100} for the *B2* simulation of Emberson, Thomas, & Alvarez (2013) (black dashed line).

2.2G64 and 2.2G32¹. The three ionized species show a dependence on the grid resolution similar to that of C_{gas} , with higher clumping factors for increasing grid size. Differently from C_{gas} and $C_{\text{R,HII},0.1}$ though, the clumping factors of helium do not seem to have reached convergence at low redshift. At high redshift a convergence would be reached only for grid sizes of at least 384^3 (although the difference between a 256^3 and a 384^3 is minimal).

From this test, we can see that even a 128^3 grid does not resolve the small scale inhomogeneities present in the gas distribution. This means that either a clumping factor should be used for each cell (which is not the aim of this paper), or higher resolution RT simulations should be run². In this case we expect a slower reionization process (smaller ionized bubbles), due to the increment in the recombination rate from the better resolved high density regions. While both the gas and ionized species clumping factors increase with grid resolution, we expect the latter to be only slightly higher than the values shown in Fig. 5, because smaller ionized regions produce lower values of clumping factors. This results in an increment milder than the one expected from an increase in gas clumping factors.

As mentioned in Emberson, Thomas, & Alvarez (2013), box size also plays an important role in determining clumping factor which is investigated in the next sub-section.

3.3.2 Dependence on Box Size

Changing the box size while keeping the same spatial resolution affects the reionization process. Here we investigate the effect of the box size on the evaluation of the clumping factor using 2.2G32, 4.4G64 and 8.8G128, which have the same sampling grid spatial resolution at different box sizes.

Fig. 6 plots the redshift evolution of C_{gas} and $C_{\text{R},i,0.1}$ for $i = \text{HII}, \text{HeII}$ and HeIII . We can see that the box size affects C_{gas} at $z < 9$. At $z \sim 4$, e.g., C_{gas} increases by ~ 20 per cent from 2.2G32 to 4.4G64, and by the same amount to 8.8G128. This is because in larger boxes at the same grid resolution, cosmic variance leads to cells with dimensionless densities higher than in smaller boxes and thus to a larger range in gas density distributions, resulting in higher C_{gas} values. As expected, the differences are more pronounced at lower redshift, when higher dimensionless densities are present.

The clumping factors of all three ionized species ($i = \text{HII}, \text{HeII}, \text{HeIII}$) show a qualitative behaviour similar to that of C_{gas} , i.e. clumping factors increasing with box size. As in the previous test, $C_{\text{R,HeII},0.1}$ shows the largest variation, with an increase in value of up to ~ 3 between each box size step at $z = 2.2$. The HeIII clumping factor shows a smaller change, with an increase of only about 1 in value between each box size step. Thus we can conclude that at a fixed spatial resolution, the box size does affect the estimate of the clumping factors, especially at low redshifts.

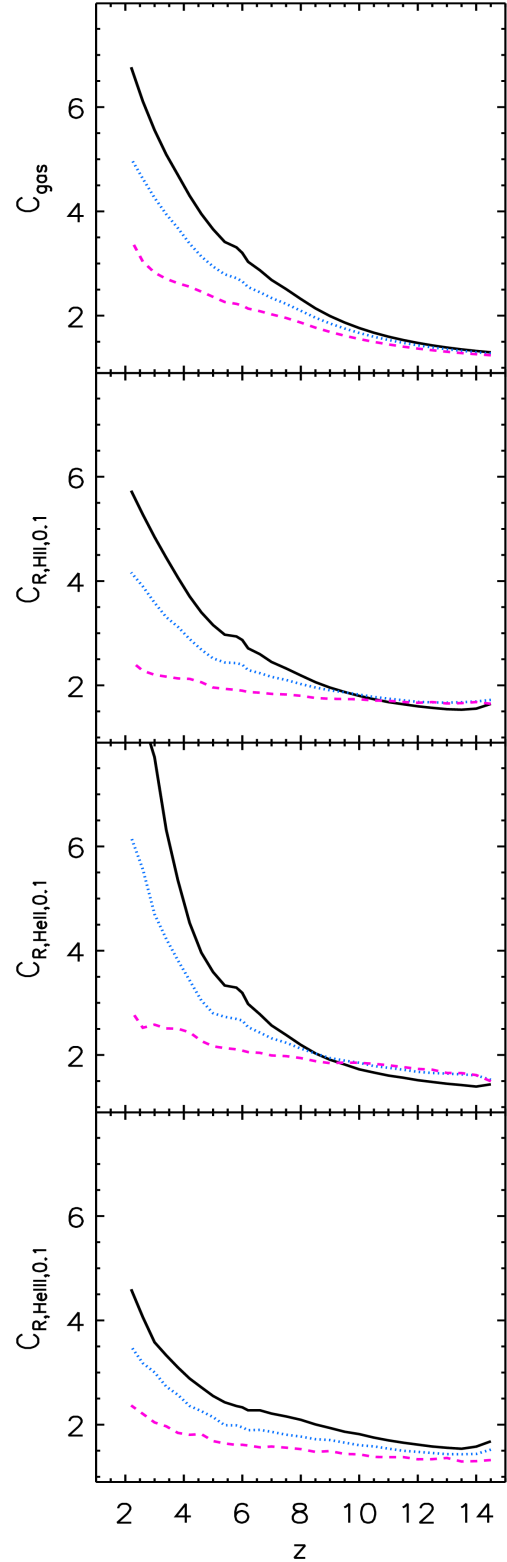


Figure 6. Redshift evolution of the clumping factor C_{gas} and $C_{\text{R},i,0.1}$ for $i = \text{HII}, \text{HeII}$ and HeIII for simulations 2.2G32 (magenta dashed line), 4.4G64 (blue dotted line) and 8.8G128 (black solid line).

¹ Higher resolution grids have been run, but not until the lowest available redshift because of the long computation time. We find though that, as for the smaller grids, the behaviour of the clumping factor of the ionized species is similar to that of the gas.

² As already mentioned, simulations with grid resolution higher than 128^3 have been run, but because of computation time they are not available for the full redshift range.

Other than resolution effects, the dimensionless density of the volume also seem to affect the calculations of clumping factors. This is studied in detail in the next sub-section.

3.4 Dependence on Mean Gas Density

Previous works have shown that the gas clumping factor correlates with the gas density (e.g. Kohler et al. 2005; McQuinn et al. 2007; Kohler, Gnedin, & Hamilton 2007). Raićević & Theuns (2011) determined that the sub-volumes within a simulation box have different gas clumping factors due to differences in the gas distribution. To investigate this further, we split 4.4G128 into eight sub-boxes with size $2.2 h^{-1}\text{Mpc}$ of 64^3 cells. Each of these sub-boxes is equivalent to 2.2G64, albeit with a different gas distribution and source properties.

From the ionization history of the different sub-boxes at the same grid resolution, we find that the higher the mean density of the sub-box is, the higher is the probability of having large ionizing sources and the faster is the reionization. This is due to the clustering of high mass objects present in the high dimensionless density regions within that volume, resulting in a larger number of ionizing photons into the IGM. Thus we can suspect that this would affect the clumping factor evolution.

Fig. 7 shows the redshift evolution of C_{gas} and $C_{\text{R},i,0.1}$ for $i = \text{HII}, \text{HeII}, \text{HeIII}$ in the eight sub-volumes. The lines for the different sub-boxes are coloured according to $\Delta_{\text{sub-box}}(z=3)$, i.e. the dimensionless density of the sub-box at $z=3$. While the qualitative behaviour of the clumping factor-dimensionless density correlation does not depend on our choice of the reference dimensionless density, the quantitative results do. It should be noted that the dimensionless density of a region is expected to vary slightly (by 20–30 per cent between $z=15$ and 3) with redshift due to the flow of gas within neighbouring sub-boxes. For the sake of clarity, the redshift evolution of the dimensionless density of the sub-boxes is shown in Fig. 8.

In the first panel of the figure, we see that C_{gas} shows a large range of values (a factor of 3–10) for the different sub-boxes at each redshift. Sub-boxes with higher dimensionless densities have a larger fraction of cells with high gas density, leading to larger gas clumping factors. The range in gas clumping factors is increasing with decreasing redshift. Note that there is a large scatter in clumping factors in sub-boxes with similar dimensionless density. This is the probable reason for the high value of clumping factors for the sub-box with dimensionless density of $\Delta_{\text{sub-box}}(z=3) = 1.03$ compared to the $\Delta_{\text{sub-box}}(z=3) = 1.19$ case.

The three ionized species $i = \text{HII}, \text{HeII}, \text{HeIII}$ exhibit very similar clumping factors at $z > 10$, while differences emerge towards lower redshift, when a dependence on the dimensionless density of the region emerges. HII has a trend similar to that of the gas, with high dimensionless density regions showing high clumping factor values. HeII exhibits a trend similar to that of HII at $z > 4$, but once HeII gets converted to HeIII (which happens faster for high density gas), the regions in which HeII remains dominant have a smaller range of densities, resulting in lower clumping factors at low redshifts. In low density regions, instead, the conversion of HeII to HeIII is slower because such areas are located further away from the sources of ionizing radiation.

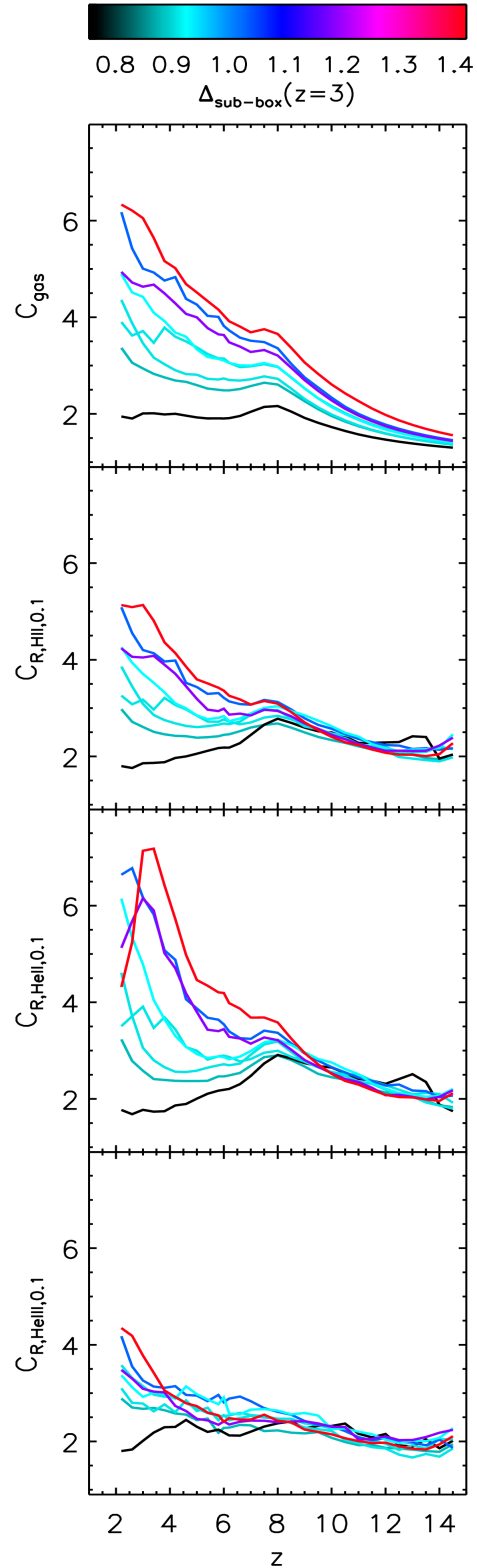


Figure 7. Evolution of the clumping factor C_{gas} and $C_{\text{R},i,x_{\text{th}}}$ for $i = \text{HII}, \text{HeII}$ and HeIII for ionization threshold $x_{\text{th}} = 0.1$ in the eight sub-boxes of 64^3 cells each from the 4.4G128 simulation. The colours refer to $\Delta_{\text{sub-box}}(z=3)$, which is the dimensionless density of the sub-box at $z=3$. The redshift evolution of the dimensionless densities of the sub-boxes has been shown in Fig. 8.

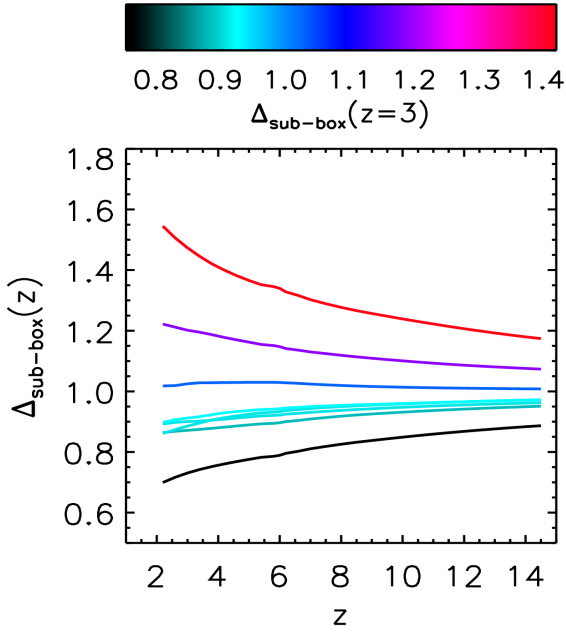


Figure 8. Evolution of the dimensionless density $\Delta_{\text{sub-box}}$ in the 8 sub-boxes of 64^3 cells each from the 4.4G128 simulation. The colours refer to $\Delta_{\text{sub-box}}(z=3)$, which is the dimensionless density of the sub-box at $z=3$. The $\Delta_{\text{sub-box}}(z=3)$ values are (bottom to top) - 0.75, 0.88, 0.91, 0.91, 0.92, 1.03, 1.19, 1.42.

The reionization within low density regions is not dominated by local sources, but rather it is influenced by the neighbouring sub-regions. This leads to a large scatter, as can be seen in the complex behaviour of $C_{\text{R,HeIII},0.1}$, which shows a general trend of mildly higher clumping factors in high density regions except for in the redshift range $4 < z < 8$, when some of the cells in the low density regions start converting from HeII to HeIII, leading to high clumping factors. They then reduce as more regions get reionized. These effects are stronger as we move to higher ionization thresholds, i.e. $x_{\text{th}} = 0.5, 0.9$, but the curves are noisier due to the small number of cells above such thresholds.

As spatial resolution of 4.4G128 is much below our best one 2.2G128, we do not quantify the trends seen in these plots but qualitatively these are the trends we expect in general.

4 CONCLUSIONS

Simulating the ionization history of a representative volume of the universe needs large box sizes, to encompass the patchy nature of the epoch of reionization and the massive ionized bubbles created towards the end of the process. High spatial/density resolution is also necessary to resolve the high-density Lyman-limit systems which control the evolution of reionization during its later stages. Since simulating large comoving volumes with very high resolution is computationally expensive, the general approach is to simulate large volumes at a lower resolution, including sub-scale clumping factors to evaluate the effect of unresolved high density regions.

Recent work (Ciardi et al. 2012) has shown that He

along with H plays an important role in determining the temperature and ionization structure of the IGM. In this work we employ similar simulations to study the different factors affecting the reionization history of the IGM and the estimation of clumping factors. We analyse a suite of simulations of box and grid sizes in the range $2.2 - 8.8 h^{-1} \text{Mpc}$ comoving and $32^3 - 448^3$, respectively.

Using 2.2G128, we calculate the clumping factor of the IGM C_i for $i = \text{gas}, \text{HII}, \text{HeII}, \text{HeIII}$. C_{gas} has values in the range $1.5 - 3$ as in Pawlik, Schaye, & van Scherpenzeel (2009). The ionized species HII and HeII converge to the values of C_{gas} at $z < 6$, while at higher redshift they reach values as high as ~ 100 . This is due to the inhomogeneous distribution of ionized gas in the simulation volume. C_{HeIII} has a qualitative behaviour similar to that of the other ionized species, but has higher values, due to the larger patchiness in the distribution of HeIII.

The extremely high values of the clumping factor mentioned above are obtained because neutral cells are also included in the calculations. When only cells above a given ionization threshold, x_{th} , are considered, the clumping factor $C_{i,x_{\text{th}}}$ of the ionized species $i = \text{HII}, \text{HeII}, \text{HeIII}$ decreases to values closer to C_{gas} . The above is true with the exception of $C_{\text{HeII},0.9}$, which increases at $z < 5$, when HeII starts to be converted to HeIII in high density regions.

Finally, the more accurate definition of clumping factor $C_{\text{R},i,x_{\text{th}}}$ is investigated, which shows that, due to the variation in the recombination coefficient with temperature and the correlation of electron density with ionization state, $C_{\text{R},i,x_{\text{th}}}$ have slightly lower values than $C_{i,x_{\text{th}}}$. The difference is the largest for HeIII clumping factors.

Grid size resolution tests on C_{gas} show that to resolve the gas density distribution (and thus C_{gas}) over the entire redshift range in our $2.2 h^{-1} \text{Mpc}$ box simulation with 256^3 gas particles, we need a sampling grid of at least 384^3 cells. C_{gas} is instead already converged at $z < 9$ in 2.2G128. We find a general trend for C_{gas} as well as for the ionized species, i.e. the clumping factors increase with increasing grid size. The evaluation of the clumping factors is also affected by the box size. We find that increasing the box size, while keeping the spatial resolution fixed, provides higher clumping factors.

The mean dimensionless density of the simulation volume plays a role in the determination of clumping factors as important as that of resolution effects. In most cases, clumping factors show a positive correlation with the mean dimensionless density, except for HeII during the later stages of reionization when it starts converting to HeIII in high density regions. This process induces a fast decrement of the clumping factor within such regions.

ACKNOWLEDGEMENTS

Many thanks to the anonymous referee for helpful comments. We thank James Bolton for providing us with the hydrodynamical simulations and for the constructive comments and suggestions throughout this work, Stuart Wyithe for the useful comments on the draft and Andreas Pawlik and Kristian Finlator for the stimulating discussions. AJD acknowledges support from and participation in the International Max Planck Research School for Astrophysics at the

Ludwig-Maximilians University. Parts of this research were conducted by the Australian Research Council Centre of Excellence for All-sky Astrophysics (CAASTRO), through project number CE110001020. LG acknowledges the support of DFG Priority Program 1573.

REFERENCES

- Barkana R., Loeb A., 2004, *ApJ*, 609, 474
 Barkana R., Loeb A., 2007, *Rep. Prog. Phys.*, 70, 627
 Bolton J. S., Haehnelt M. G., 2007, *MNRAS*, 382, 325
 Ciardi B., Ferrara A., Marri S., Raimondo G., 2001, *MNRAS*, 324, 381
 Ciardi B., Ferrara A., 2005, *Space Sci. Rev.*, 116, 625
 Ciardi B., Bolton J. S., Maselli A., Graziani L., 2012, *MNRAS*, 423, 558
 Emberson J. D., Thomas R. M., Alvarez M. A., 2013, *ApJ*, 763, 146
 Fan X., et al., 2006, *AJ*, 131, 1203
 Finlator, K., Oh, S. P., Özel, F., & Davé, R. 2012, *MNRAS*, 427, 2464
 Giroux M. L., Shapiro P. R., 1996, *ApJS*, 102, 191
 Gnedin N. Y., Ostriker J. P., 1997, *ApJ*, 486, 581
 Graziani L., Maselli A., Ciardi B., 2013, *MNRAS*, 431, 722
 Haardt F., Madau P., 2001, *Clusters of Galaxies and the High Redshift Universe Observed in X-rays*
 Haardt F., Madau P., 2012, *ApJ*, 746, 125
 Iliev I. T., Scannapieco E., Shapiro P. R., 2005, *ApJ*, 624, 491
 Iliev I. T., Mellema G., Shapiro P. R., Pen U.-L., 2007, *MNRAS*, 376, 534
 Kurov A. A., Gnedin N. Y., 2014, *ApJ*, 787, 146
 Kohler K., Gnedin N. Y., Miralda-Escudé J., Shaver P. A., 2005, *ApJ*, 633, 552
 Kohler K., Gnedin N. Y., Hamilton A. J. S., 2007, *ApJ*, 657, 15
 Komatsu E., et al., 2011, *ApJS*, 192, 18
 Lacey C., Cole S., 1994, *MNRAS*, 271, 676
 McQuinn M., Lidz A., Zahn O., Dutta S., Hernquist L., Zaldarriaga M., 2007, *MNRAS*, 377, 1043
 McQuinn M., Oh S. P., Faucher-Giguère C.-A., 2011, *ApJ*, 743, 82
 Madau P., Haardt F., Rees M. J., 1999, *ApJ*, 514, 648
 Maselli A., Ferrara A., Ciardi B., 2003, *MNRAS*, 345, 379
 Maselli A., Ciardi B., Kanekar A., 2009, *MNRAS*, 393, 171
 Miralda-Escudé J., Haehnelt M., Rees M. J., 2000, *ApJ*, 530, 1
 Morales M. F., Wyithe J. S. B., 2010, *ARA&A*, 48, 127
 Osterbrock D. E., 1989, *Astrophysics of Gaseous Nebulae and Active Galactic Nuclei*. University Science Books, Mill Valley, CA
 Padmanabhan, T. 1993, *Structure Formation in the Universe*, by T. Padmanabhan, pp. 499. ISBN 0521424860. Cambridge, UK: Cambridge University Press, June 1993.
 Partl A. M., Maselli A., Ciardi B., Ferrara A., Müller V., 2011, *MNRAS*, 414, 428
 Pawlik A. H., Schaye J., van Scherpenzeel E., 2009, *MNRAS*, 394, 1812
 Pawlik A. H., Schaye J., 2011, *MNRAS*, 412, 1943

- Pierleoni M., Maselli A., Ciardi B., 2009, *MNRAS*, 393, 872
 Raičević M., Theuns T., 2011, *MNRAS*, 412, L16
 Schaye J., 2001, *ApJ*, 559, 507
 Shull J. M., Harness A., Trenti M., Smith B. D., 2012, *ApJ*, 747, 100
 So G. C., Norman M. L., Reynolds D. R., Harkness R. P., 2014, *ApJ*, 789, Q11 149
 Springel V., 2005, *MNRAS*, 364, 1105
 Telfer R. C., Zheng W., Kriss G. A., Davidsen A. F., 2002, *ApJ*, 565, 773
 Trac H., Cen R., 2007, *ApJ*, 671, 1
 Wyithe J. S. B., Loeb A., 2004, *Nature*, 432, 194

APPENDIX A: IONIZATION HISTORY FOR RESOLUTION TEST SIMULATIONS

In this section, for the sake of clarity, we show how the grid and box size affect the ionization history. Fig. A1 shows the fraction of HII, HeII and HeIII for 2.2G128, 2.2G64 and 2.2G32. All simulations have the same hydrodynamic resolution but different grid size. The general trend is that of a faster reionization of the volume with a decreasing grid size, due to the lower rate of recombination in low resolution simulations, showing the necessity of using a clumping factor in simulations which under-resolve the gas density distribution. This trend is inverted for x_{HeII} at $z < 8$, where the conversion of HeII to HeIII dominates over the single ionization of HeI.

In Fig. A2, we plot the fraction of HII, HeII and HeIII for 2.2G32, 4.4G64 and 8.8G128. These simulations have equal gridding resolution but different box sizes. For HII and HeIII, the presence of stronger sources, due to cosmic variance, lead to higher ionization values in larger boxes at $z > 12$. As the density field evolves at lower redshifts ($6 < z < 12$), the effect of stronger ionizing sources is mitigated by the contribution of higher recombination rates in the high density cells around these sources. Eventually at $z < 6$, a strong rise in emissivity causes the ionization fractions in large boxes to increase rapidly, especially for HeIII. In the case of x_{HeII} , the high conversion rate of HeII to HeIII in large boxes leads to low x_{HeII} at all redshifts. But as the conversion of HeIII to HeII increase at intermediate redshifts ($6 < z < 12$), the recombination of HeII also increase causing the trend to stay the same till $z < 6$, after which the high emissivity causes the ionization of HeII to become the dominant factor and thus reversing the trend. It should be noted that in general the effect of box size is stronger for the He component of the gas, while the H is only mildly affected.

Therefore, we conclude that both grid size and box size play an important role in determining the ionization history of a volume which in turn affect the clumping factor values.

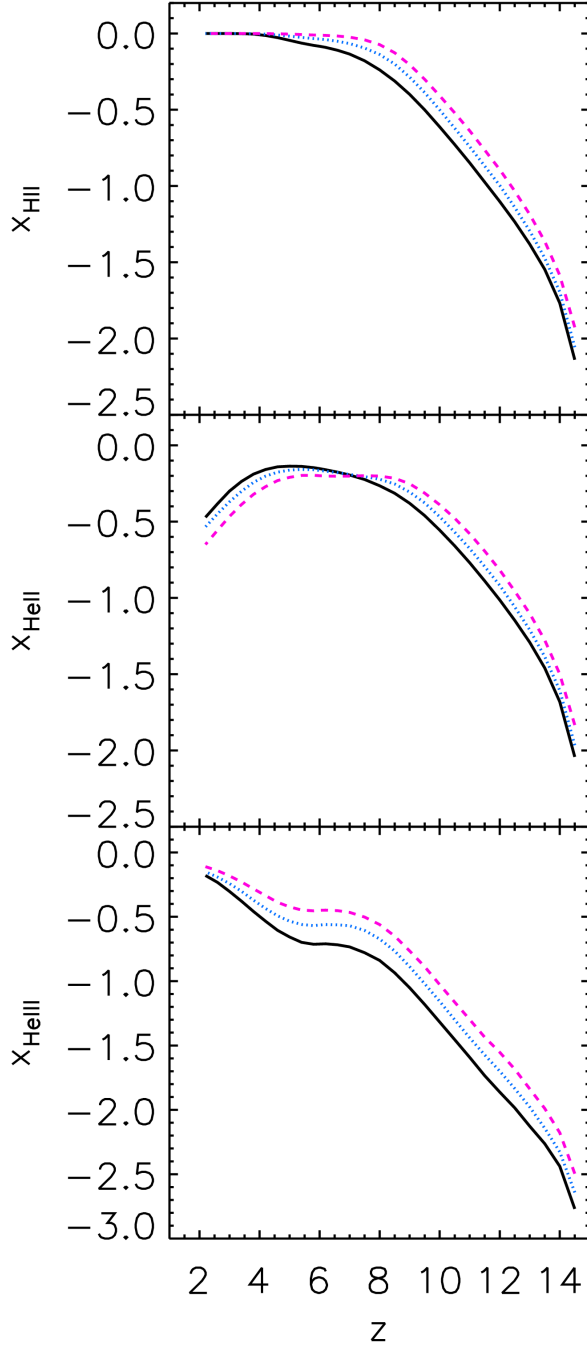


Figure A1. Redshift evolution of the ionization fractions x_i for $i = \text{HII}$, HeII and HeIII for the simulations 2.2G128 (black solid line; reference), 2.2G64 (blue dotted line) and 2.2G32 (magenta dashed line).

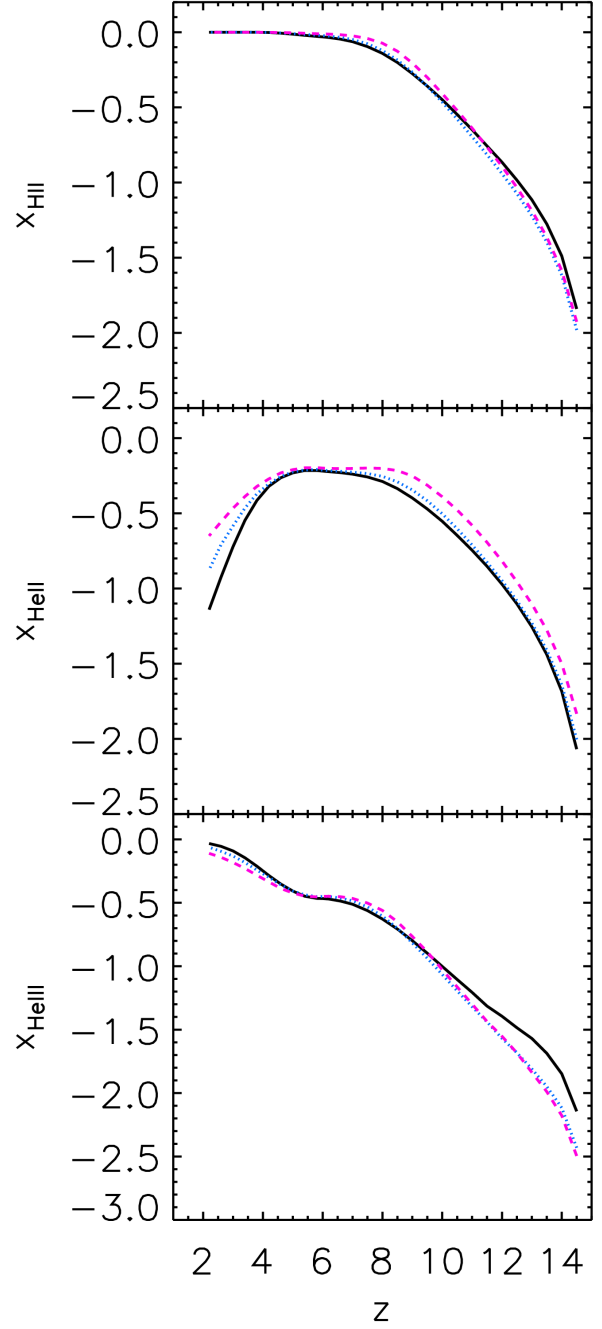


Figure A2. Redshift evolution of the ionization fractions x_i for $i = \text{HII}$, HeII and HeIII for simulations 2.2G32 (magenta dashed line), 4.4G64 (blue dotted line) and 8.8G128 (black solid line).